Global trends of the electric dipole polarizability from shell-model calculations

José Nicolás Orce [1,2,*] Cebo Ngwetsheni [1] and B. Alex Brown [3]

[1]*Department of Physics & Astronomy, University of the Western Cape, P/B X17, Bellville 7535, South Africa*

[2]*National Institute for Theoretical and Computational Sciences (NITheCS), Stellenbosch, South Africa*

[3]*Department of Physics and Astronomy, and the Facility for Rare Isotope Beams, Michigan State University, East Lansing, Michigan 48824-1321, USA*

(Received 25 July 2023; accepted 13 September 2023; published 12 October 2023)

Shell-model calculations of the electric dipole ($E1$) polarizability have been performed for the ground state of selected p- and sd-shell nuclei, substantially advancing previous knowledge. Our results are slightly larger compared with the somewhat more scattered photoabsorption cross-section data, albeit agreeing with *ab initio* calculations at shell closures and presenting a smooth trend that follows the leptodermous approximation provided by the finite-range droplet model (FRDM). The total $E1$ strengths also show an increasing trend proportional to the mass number which follows from the classical oscillator strength (TRK) sum rule for the $E1$ operator. The enhancement of the energy-weighted sum over $E1$ excitations with respect to the TRK sum rule arises from the use of experimental single-particle energies and the residual particle-hole interaction.

DOI: 10.1103/PhysRevC.108.044309

I. MOTIVATION

The ability for a nucleus to be polarized is driven by the dynamics of the isovector giant dipole resonance (GDR) [1], which can be characterized macroscopically as the collective motion of interpenetrating proton and neutron fluids out of phase [2–4], and microscopically, through the shell-model (SM) interpretation of a system of independent nucleons plus configuration mixing or the superposition of one particle one hole (1p-1h) excitations [5–8]. This collective motion can be related to the nuclear symmetry energy $a_{\rm sym}(A)(\rho_N - \rho_Z)^2/\rho_A$—as defined in the Bethe–Weizsäcker semi-empirical mass formula [9,10]—acting as a restoring force [11], where $a_{\rm sym}(A)$ is the symmetry energy coefficient, A the atomic mass number, $A = N + Z$, and ρ_N, ρ_Z, and ρ_A the neutron, proton, and total fluid densities, respectively.

Within the hydrodynamic model, the dipole polarizability α_{E1} is directly proportional to $A^{5/3}$ and inversely proportional to $a_{\rm sym}(A)$ [2,12],

$$\alpha_{E1} = \frac{P}{E} = \frac{e}{E}\int_V \rho' z^2 dV = \frac{e^2R^2A}{40a_{\rm sym}(A)}, \tag{1}$$

where E is the magnitude of an electric field along the positive z axis, P the dipole moment with density $e\rho' z^2$, $\rho' = eE\rho_A/[8a_{\rm sym}(A)]$, and R the radius of a nucleus with a well-defined surface, $R = 1.2A^{1/3}$ fm.

Complementary, using nondegenerate perturbation theory, α_{E1} is defined in terms of the energy-shift of the nuclear levels arising from the quadratic Stark effect [13], i.e., $\Delta E = -\frac{1}{2}\alpha E^2$, and can be determined for ground states with an arbitrary initial angular momentum J_i using the inverse energy-weighted sum rule [14],

$$\alpha_{E1} = \frac{2e^2}{2J_i+1}\sum_n \frac{|\langle i \parallel \hat{E1} \parallel n\rangle|^2}{E_n - E_i} = \frac{9\hbar c}{8\pi^3}\sigma_{-2}, \tag{2}$$

where $2J_i + 1$ is the normalization constant arising from the Wigner-Eckart theorem [15,16], and the sum extends over all $|n\rangle$ intermediate states connecting the initial ground state $|i\rangle$ with electric dipole or $E1$ transitions. The σ_{-2} value is the (-2) moment of the total photoabsorption cross section, $\sigma_{total}(E_\gamma)$, defined as [17,18],

$$\sigma_{-2} = \int_0^{E_\gamma^{\rm max}} \frac{\sigma_{total}(E_\gamma)}{E_\gamma^2} dE_\gamma, \tag{3}$$

which is generally integrated between particle threshold and the available upper limit for monochromatic photons, $E_\gamma^{\rm max} \approx$ 20–50 MeV [19]. An upper limit of $E_\gamma^{\rm max} \approx 50$ MeV approximates the σ_{-2} asymptotic value for light and medium-mass nuclei [20]. Magnetic polarizability contributions [21] are not considered here but may be relevant for ^{6}Li and ^{7}Li [22].

The bulk of knowledge on how atomic nuclei polarize arises from photoabsorption cross-section data [19,23,24], where most of the absorption (and emission) of photons is provided by the GDR [25]. Data predominantly involve photoneutron cross sections—although photoproton contributions are dominant for some light and $N = Z$ self-conjugate nuclei [26]—and mainly concern the ground states of nuclei. To a much lesser extend, α_{E1} has been determined from several experiments using radioactive ion beams [27], inelastic proton scattering [28–32] and virtual photons [33].

Other phenomena that can contribute to σ_{-2} values are the pygmy dipole resonance (PDR) [52–56]—an out-of-phase oscillation of the valence nucleons against the core—and

*Corresponding author: jnorce@uwc.ac.za; coulex@gmail.com; http://nuclear.uwc.ac.za.

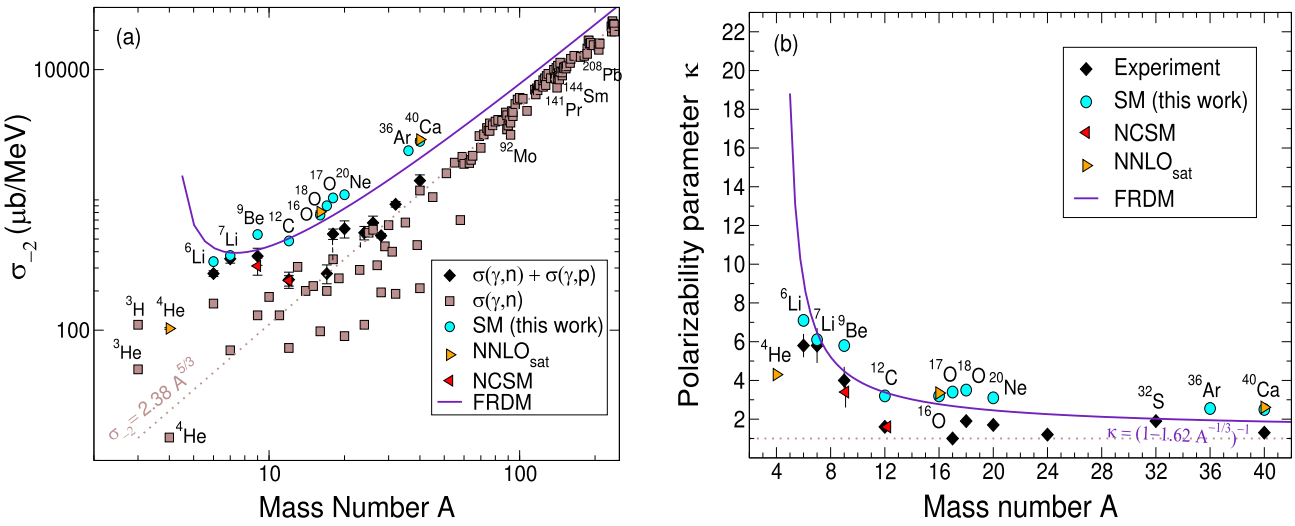

FIG. 1. Experimental and calculated σ_{-2} (left) and κ (right) values for the ground states of selected p- and sd-shell nuclei. Data points (square and diamonds) arise from available photoabsorption cross sections [19,22,34,35,35–47]. The theoretical results are taken from Ref. [48] (coupled-cluster with $\mathrm{NNLO_{sat}}$) and Refs. [49,50] (NCSM). The WBP and FSU SM calculations (circles) are from the current work. For comparison, the hydrodynamic-model prediction for $\kappa = 1$ in Eq. (4) is shown by dotted lines together with the leptodermous trend [Eq. (6)] given by the FRDM symmetry energy coefficients, $S_v = 30.8$ MeV, $S_s/S_v = 1.62$ (solid lines) [51].

low-energy nuclear resonances arising from cluster formation [57–59]. The PDR has been identified in light nuclei with neutron excesses [41,52,53,56,60,61]—being ^{13}C where the "pygmy resonance" was originally termed [56]—but has never been observed along the $N = Z$ line of stability. Estimates suggest a contribution of about 5%–10% to σ_{-2} values, similar to those found in stable neutron-rich nuclei [54]. A larger contribution is expected as N increases and approaches the neutron drip line [62]. An additional contribution could potentially arise from the low-energy enhancement (LEE) of the photon-strength function [63–70], although $^{43-45}$Sc are the lightest nuclei where it has been identified [63,64].

Photoneutron cross-section data for $A \gtrapprox 50$ nuclei—where neutron emission is generally the predominant decay mode—show a smooth trend of σ_{-2} values in the left panel of Fig. 1 (dotted line), following the empirical power-law formula [71,72],

$$\sigma_{-2}(A) = 2.38\kappa A^{5/3}\ \mu\mathrm{b/MeV}, \tag{4}$$

where κ accounts for deviations from the actual GDR effects to that predicted by the hydrodynamic model [2,12]. Here, all quoted σ_{-2} and κ values are related to Eq. (4). Deviations from the smooth trend ($\kappa = 1$) arise for loosely bound light nuclei ($\kappa > 1$) [71] and semimagic nuclei ($\kappa < 1$) [68–70], where the extra stability of shell closures may hinder polarization.

In this work, we investigate α_{E1} for ground states of nuclei within the p and sd shells by performing novel $1\hbar\omega$ SM calculations—following Eq. (2)—with the $p - sd$ Hamiltonian of Warburton and Brown (WBP) and the Florida State University (FSU) Hamiltonians. We further explore deviations from the smooth trend ($\kappa = 1$) predicted by the hydrodynamic model in Eq. (4), and compare our results with available photoabsorption cross-section data [73,74], sums of $E1$ strengths and the classical oscillator strength sum rule for the $\hat{E}1$ operator.

II. SHELL-MODEL CALCULATIONS

Shell-model calculations of the $E1$ polarizability are demanding since they normally involve hundreds of $E1$ matrix elements and high-performance computing. Priorly, SM calculations of κ values for ground states have been carried out—following Eqs. (2) and (4)—in ^{9,10}Be [49] and ^{12}C [50] using the no-core shell-model (NCSM) with the CD-Bonn $2N$ and chiral effective-field theory (χEFT) $2N + 3N$ forces [77–82], $N_{\max} = 4$ basis sizes for natural and $N_{\max} = 5$ for unnatural parity states. These *ab initio* calculations included $E1$ matrix elements from all the transitions connecting about 301^- states up to 30 MeV in ^{10}Be and ^{12}C, and $E1$ contributions from about 100 intermediate $1/2^+$, $3/2^+$, and $5/2^+$ states in ^{9}Be. For the ground states of ^{9}Be and ^{12}C, values of $\kappa(\mathrm{g.s.}) = 3.4(8)$ and $\kappa(\mathrm{g.s.}) = 1.6(2)$ were predicted, respectively, in agreement with photoabsorption cross-section data [12,34,40]. Additional NCSM calculations of α_{E1} values have been performed in ^{3}H, ^{3}He, and ^{4}He by Stetcu and collaborators using directly the Schrödinger equation and χEFT interactions [83].

In the present work, $1\hbar\omega$ SM calculations of the ground-state $E1$ polarizability have been carried out using the OXBASH code [84] with the Warburton and Brown (WBP) [85] and Florida State University (FSU) [86–88] Hamiltonians within the $spsd$ pf model space. For nuclei near ^{16}O, the FSU Hamiltonian [86–88] is the same as the WBP Hamiltonian from Ref. [85]. The single-hole energies are fixed to the experimental separation energies between the ^{16}O ground state and states in ^{15}O; -22.11 and -15.54 MeV for $0p_{1/2}$ and $0p_{3/2}$, respectively. The single-particle states are determined by the separation energies between states in ^{17}O and the ^{16}O ground

TABLE I. Experimental and calculated σ_{-2} (columns 3 and 4) and κ (columns 7 and 8) values of ground states in selected p- and sd-shell nuclei. Experimental data arise from available photoabsorption cross sections. Previous calculations (column 9) are listed for comparison. All quoted σ_{-2} and κ values presented in this work are related to Eq. (4). Shell model calculations below ^{17}O are from the WBP interaction, whereas for $A \geqslant 17$ we quote the values from the FSU interaction. Slightly smaller values are determined with the WBP interaction in the middle and end of the sd shell.

Nucleus	J^π	$\sigma_{-2}^{\text{expt}}$ μb/MeV	σ_{-2}^{SM} μb/MeV	$E_{\text{max}}^{\text{SM}}$ MeV	$\sum_n B(E1_n)^{\text{SM}}$ e^2 fm^2	κ^{expt}	κ^{SM}	κ^{previous}
^{6}Li	1^+_1	272(14) [22,35–37]	336	34.0	1.7	5.8(6)	7.1	
^{7}Li	$3/2^-_1$	353(26) [22,38,39]	374	47.0	1.9	5.8(9)	6.1	
^{9}Be	$3/2^-_1$	370(55) [34]	542	58.3	2.5	4.0(8)	5.8	3.4(8) [49]
^{12}C	0^+_1	244(35) [40]	484	65.1	2.9	1.6(2)	3.2	1.6(2) [50]
^{16}O	0^+_1	616(90) [40]	765	25.9	4.5	2.5(4)	3.2	3.4(1) [48]
^{17}O	$5/2^+_1$	272(45) [41,42]	901	35.2	4.7	1.2(2)	3.4	
^{18}O	0^+_1	547(50) [43]	1035	44.3	5.3	1.9(3)	3.5	
^{20}Ne	0^+_1	600(90) [44,45]	1095	47.0	6.3	1.7(3)	3.1	
^{24}Mg	0^+_1	559(66) [46,47]	1132	42.2	5.9	1.2(2)	2.4	
^{36}Ar	0^+_1		2384	31.8	11.6		2.6	
^{40}Ca	0^+_1	1405(150) [75,76]	2813	24.5	13.8	1.3(2)	2.5	2.6(1) [48]

state, as used in the USDB Hamiltonian [89], −3.93, −3.21, and 2.11 MeV for $0d_{5/2}$, $1s_{1/2}$, and $0d_{3/2}$, respectively. The energies of the pure 1p-1h states range from 11.6 to 24.1 MeV.

The two-body matrix elements (TBME) involving both $0p$ and $0d$-$1s$ in the WBP Hamiltonian for nuclei near ^{16}O were obtained from a realistic potential model that contains a fixed one-pion exchange part, plus adjusted strengths of central, spin-orbit and tensor contributions from one-boson exchange [see Eq. (4) in Ref. [85]]. There is no explicit velocity dependence [90]. The parameters were obtained by fitting to the data given in Table IV of Ref. [85]. The FSU Hamiltonian starts with the WBP Hamiltonian, and then adjusts linear combinations of TBME of the type $\langle 0d\text{-}1s, 0f\text{-}1p, J, T \mid V \mid 0d\text{-}1s, 0f\text{-}1p, J, T\rangle$ to fit the data shown in Fig. 6 of Ref. [86]—which include particle-hole states originating from cross-shell excitations that give rise to intruder states—and is built upon tuning the monopole terms across the shell gaps $N = 8$ and $N = 20$ to reproduce the experimental data.

The general procedure in our SM calculations is calculating all $E1$ matrix elements following Eq. (2). For even-even nuclei, we calculate $\langle 0^+_1 \parallel \hat{E1} \parallel 1^-_n\rangle$ $E1$ matrix elements connecting the ground state with up to 1000 intermediate 1^-_n isovector excitations with a maximum calculated energy $E_{\text{max}}^{\text{SM}}$ listed in Table I, which include the GDR region. Similarly, we calculate all possible $E1$ matrix elements from the various intermediate states for odd-even and odd-odd nuclei. SM calculations for ^{28}Si and ^{32}S were not feasible because of limiting computing power and accuracy.

Isospin selection rules for $E1$ transitions [91] have to be considered according to the corresponding Wigner $3j$ symbols; ergo, isovector contributions for $N = Z$ self-conjugate nuclei [$T_z = (N - Z)/2 = 0$] arise only from $\Delta T = 1$ transitions, whereas both $\Delta T = 0, 1$ isovector transitions have to be considered otherwise. Such an isospin splitting of $E1$ strengths is shown in Fig. 2 for ^{17}O (top) and ^{18}O (bottom),

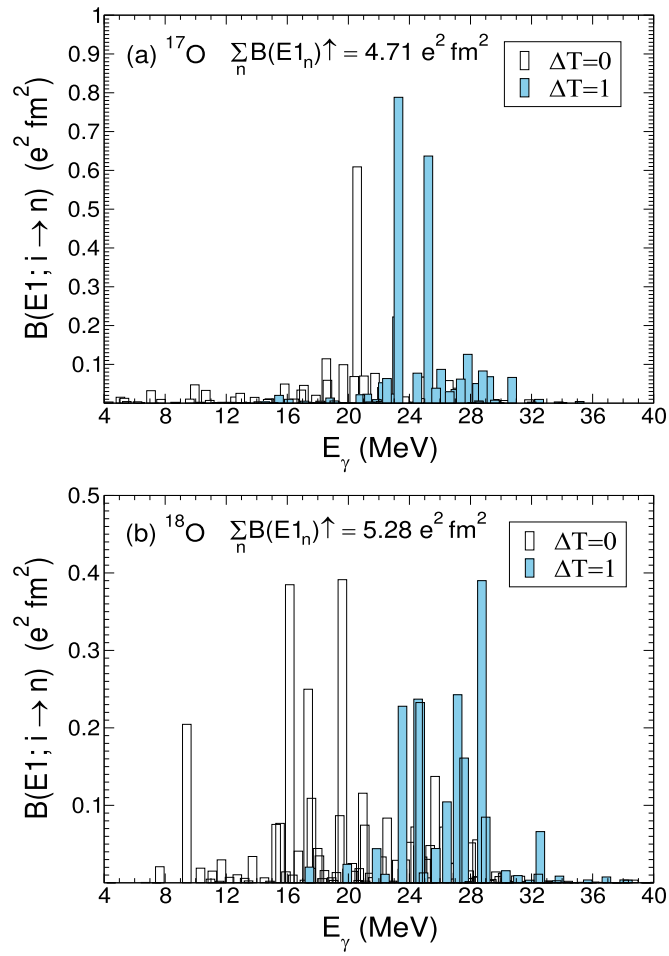

FIG. 2. Calculated $B(E1; 0^+_1 \rightarrow 1^-_n)$ isovector distribution as a function of transition energies for ^{17}O and ^{18}O for both $\Delta T = 0$ and $\Delta T = 1$ transitions.

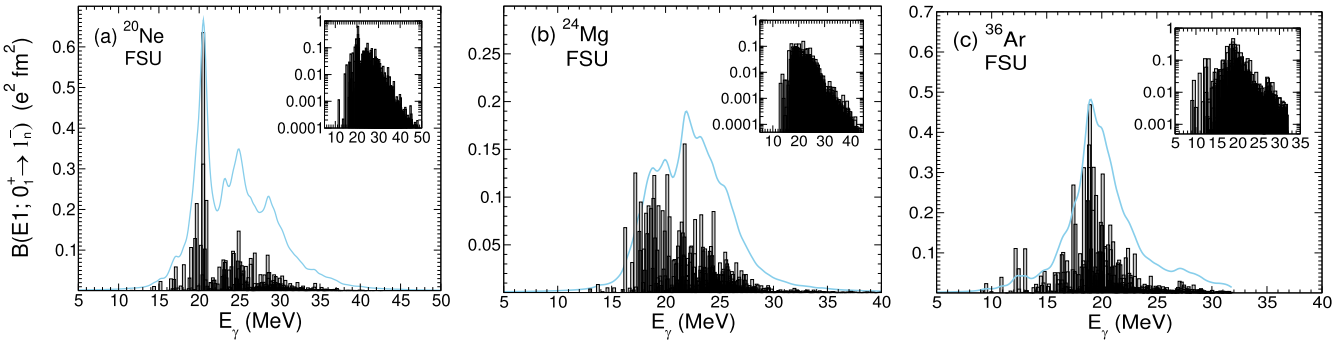

FIG. 3. Calculated $B(E1; 0_1^+ \rightarrow 1_n^-)$ isovector distribution ($\Delta T = 1$) as a function of transition energies for ^{20}Ne, ^{24}Mg, and ^{36}Ar. The light blue curves represent the strength distributions folded with a Lorentzian function with 1-MeV width, and illustrate the spreading of the strength.

where $B(E1_n)$ is the reduced transition probability connecting the ground state $|i\rangle$ with each final state $|n\rangle$ [92],

$$B(E1_n) = B(E1; i \rightarrow n) = \frac{1}{2J_i + 1} |\langle n||\hat{E1}||i\rangle|^2. \quad (5)$$

Isospin mixing at high-excitation energies is less than 5% in the GDR region [57,93,94].

Moreover, $E1$ effective charges are not required since all the $E1$ matrix elements are calculated in the full $1\hbar\omega$ model space, i.e., as shown in Fig. 3, we do a full and fully converged $1\hbar\omega$ calculation of 1p-1h excitations that occur between major shells. Dipole excitations far above the GDR region have a negligible effect. Although $3\hbar\omega$ 1p-1h matrix elements are all zero in the harmonic oscillator (H.O.), novel SM calculations by Sieja in the neon isotopes show that possible admixtures with $1\hbar\omega$ 1p-1h + 2p-2h transitions may suppress the $E1$ strength by about 15% [95,96].

Removing spurious states is of particular relevance for $E1$ transitions in $N \approx Z$ nuclei because the motion of a particle involves the recoil of the rest of the nucleus, with the total center of mass remaining at rest [92]. Following the Gloeckner-Lawson method [97], the center-of-mass Hamiltonian incorporated in OXBASH conveniently pushes away 1p-1h spurious states involving $0s$ to $0p$, $0p$ to $0d1s$, and $0d1s$ to $0f1p$, and decouples them from intrinsic excitations [98]. Table I and Fig. 1 show the calculated $\sigma_{-2}^{\rm SM}$ and $\kappa^{\rm SM}$ values for the ground states of selected p- and sd-shell nuclei. For comparison, other theoretical results are also presented together with available photoabsorption cross-section measurements of $\sigma_{-2}^{\rm expt}$ and $\kappa^{\rm expt}$ values. It should be noted that previous *ab initio* calculations of α_{E1} in ^{16}O and ^{40}Ca [48] using integral transforms and the coupled-cluster method with the NNLO$_{\rm sat}$ interaction (right triangles in Fig. 1) agree with our results.

III. RESULTS AND DISCUSSION

Pronounced deviations from hydrodynamic-model estimates (dotted $\kappa = 1$ lines in Fig. 1) are calculated for the ground states of ^{6,7}Li and ^{9}Be, with slightly larger σ_{-2} and κ values than those found experimentally. Such deviations from the GDR effect are not surprising considering the fragmentation of the GDR spectrum into different 1p-1h states [57], which include the possibility of α cluster configurations [99,100] and the virtual breakup into the continuum [101,102]. The latter even led Smilansky, Weller, and coworkers to suggest that the main contribution to the polarizability in ^{7}Li may not actually be the GDR, but instead the virtual breakup into the α-t continuum. The rise of cluster structures in ^{6,7}Li, ^{9}Be, as well as ^{17}O can be pinned down to the extra loosely bound or slightly unbound particle [103,104]—whose wave function extends far apart from the α-cluster configurations, i.e., $\alpha + d$, $\alpha + t$, $2\alpha + n$, $4\alpha + n$, respectively—as inferred from the dipole resonances observed at relatively low-excitation energies [41,58,59]. Deviations from the hydrodynamic model in self-conjugate $N = Z$ nuclei could also arise because of cluster formation [100,105–110] and/or the missing admixtures with $1\hbar\omega$ 1p-1h + 2p-2h transitions [95,96]. Despite slightly larger values are generally calculated compared with measurements, the right panel of Fig. 1 present similar theoretical and experimental trends of κ values, and suggest that the bulk of these effects are implicitly incorporated in the phenomenological Hamiltonians. The larger $\kappa^{\rm SM}$ value in ^{17}O is about three times larger than the experimental one and deserves further investigation as a substantially larger $\kappa = 8.4(6)$ has also been experimentally determined for its first excitation [111].

Interestingly, the overall smooth trend of $\sigma_{-2}^{\rm SM}$ and $\kappa^{\rm SM}$ values shown in Fig. 1 can be independently correlated with the leptodermous approximation ($A^{-1/3} \ll 1$) of the symmetry energy [71,112,113],

$$a_{\rm sym}(A) = S_v \left(1 - \frac{S_s}{S_v} A^{-1/3}\right), \quad (6)$$

where S_v is the volume symmetry-energy coefficient and S_s/S_v the surface-to-volume ratio for finite nuclei.

The set of S_v and S_s parameters that best reproduce the overall trends in Fig. 1 is provided by the finite-range droplet model (FRDM) [114], i.e., the combination of the finite-range droplet macroscopic model and the folded-Yukawa single-particle microscopic model [51]. The leptodermous trends for σ_{-2} and κ are shown in Fig. 1(solid lines) and determined by combining the FRDM parameters ($S_v = 30.8$ MeV and $S_s/S_v = 1.62$) with Eqs. (1), (2), and (4),

$$\sigma_{-2}(A) = \frac{2.35A^2}{A^{1/3} - 1.62}, \quad (7)$$

$$\kappa(A) \approx \frac{1}{1 - 1.62A^{-1/3}}, \quad (8)$$

TABLE II. Classical $S(E1)^{\rm TRK}$ [Eq. (10)] and $S(E1)^{\rm SM}$ [Eq. (10)] sum rules. The H.O. energy $\hbar\omega$ in column 4 is fit to reproduce the rms charge radii—instead of using $\hbar\omega = 41A^{-1/3}$ MeV—providing $\Sigma B(E1_n)^{rms}$ for $N = Z$ nuclei without particle-hole interactions. The $f_{\rm GDR}$ ratio indicates the fraction of the TRK sum rule exhausted for each nucleus.

Nucleus	$S(E1)^{\rm TRK}$ e^2 fm^2 MeV	$S(E1)^{\rm SM}$ e^2 fm^2 MeV	$\hbar\omega$ MeV	$\Sigma B(E1_n)^{rms}$ e^2 fm^2	$f_{\rm GDR}$
^{6}Li	22.2	36.2	11.74	1.89	1.63
^{7}Li	25.4	42.5	13.71	1.85	1.67
^{9}Be	32.9	51.1	13.51	2.43	1.55
^{12}C	44.4	71.2	15.66	2.84	1.60
^{16}O	59.2	106.3	13.26	4.47	1.80
^{17}O	62.7	106.6	13.35	5.87	1.70
^{18}O	65.8	117.7	12.51	5.26	1.79
^{20}Ne	74.0	149.5	11.88	6.23	2.02
^{24}Mg	88.8	128.0	12.62	7.04	1.44
^{36}Ar	133.2	235.5	11.05	12.05	1.78
^{40}Ca	148.0	274.8	10.77	13.74	1.86

which characterize the enhancement observed for light nuclei. Additional sets of S_v and S_s/S_v parameters are discussed in Ref. [33] and references therein, albeit presenting larger deviations from the overall trends of SM calculations and data.

Further support of SM calculations may arise from the calculated sum of $E1$ strengths, $\sum_n B(E1_n)$, shown in Tables I and II. The $B(E1_n)$ values are calculated with H.O. radial wave functions. The simplest approximation is $\hbar\omega = 41A^{-1/3}$ MeV for uncorrelated or independent-particle motion of the nucleons. That is, when there is no particle-hole interaction, the 1^-, $T = 1$ GDR is split among all possible 1p-1h states at an energy of $E_{\rm GDR} = 1\hbar\omega$. The total $E1$ strength then obeys the classical oscillator strength or TRK sum rule [92,115–118],

$$S(E1)^{\rm TRK} = E_{\rm GDR}\,\Sigma B(E1_n) = 14.8\frac{NZ}{A}\ \text{MeV}\,e^2\,\text{fm}^2. \quad (9)$$

For $N = Z$, $S(E1)^{\rm TRK} = 3.7A$ MeV e^2 fm^2, and $\Sigma B(E1_n)^{\rm TRK} = 0.090A^{4/3}$ e^2 fm^2 when $E_{\rm GDR} = 1\hbar\omega$. For our calculations we use the $\hbar\omega$ required to reproduce the rms charge radii [119], which are listed in Table II—in closer agreement with Blomqvist and Molinari's $\hbar\omega = 45A^{-1/3} - 25A^{-2/3}$ MeV [120]—together with the corresponding $\Sigma B(E1_n)^{rms}$ for $N = Z$. For example, for $\hbar\omega = 13.26$ MeV in ^{16}O, there are five 1p-1h 1^-, $T = 1$ states with $\Sigma B(E1_n) = 4.47\ e^2$ fm^4.

When the particle-hole interaction is turned on, the 1p-1h states mix and are pushed up in energy forming the collective dipole resonance. In our 1p-1h model the summed $B(E1)$ strength remains the same after mixing. The resulting SM energy-weighted sum over $E1$ excitations up to $E^{\rm SM}_{\rm max}$ is then given by

$$S(E1)^{\rm SM} = \sum_n^{E^{\rm SM}_{\rm max}} E^{\rm SM}_n B(E1_n)^{\rm SM}. \quad (10)$$

Our results for $S(E1)^{\rm SM}$ are presented in Table II, together with the fraction of the TRK sum rule exhausted for each nucleus,

$$f_{\rm GDR} = \frac{S(E1)^{\rm SM}}{S(E1)^{\rm TRK}}. \quad (11)$$

The $\sum_n B(E1_n)^{\rm SM}$ values are presented in Table I. In general, $f_{\rm GDR}$ values exceedingly exhaust the TRK sum rule by approximately 1.5–2 times. In ^{16}O, the 1p-1h states are formed by linear combinations of the five possible excitations. The strongest state that comes at 23.6 MeV contains 89% of the $E1$ strength. The TRK sum is enhanced by a factor of $23.6/13.3 = 1.8$. For ^{24}Mg, we are missing some of the $E1$ strength in the lowest 20001^- $T = 1$ states, presenting the smallest $f_{\rm GDR}$ value of 1.44.

Below ^{16}O one includes both $0s$ to $0p$ and $0p$ to $0d$-$1s$. Above ^{16}O and below ^{40}Ca one includes $0p$ to $0d$-$1s$ and $1d$-$0s$ to $0f$-$1p$. For these nuclei the strength becomes more fragmented—as shown in Fig. 3[1]—due to coupling with 1^- states that are built on other other (nonclosed-shell) positive-parity states. For example, in ^{20}Ne there are 1525 nonspurious 1^-, $T = 1$ states (one can make spurious 1^-, $T = 1$ states by coupling spurious 1^-, $T = 0$ states to positive parity states with $T = 1$). As expected, in ^{20}Ne there is a negligible $E1$ strength at low excitation energies below $\approx$14 MeV, in agreement with recent calculations using the microscopic configuration-interaction method [96]. The same happens for ^{24}Mg. Nonetheless, some $E1$ strength starts developing at low energies in ^{36}Ar as the $Z = N = 20$ shell closures approach.

The TRK sum is increased due to the increase in energy of the GDR from $1\hbar\omega$. In these SM calculations, the TRK enhancement factor comes from using realistic single-particle energies (as given above for ^{16}O) and the attractive particle-hole interaction, which is dominated by the central part of the potential.

The centroid of our calculated GDR is systematically higher that those obtained from (p, p') experiments for sd shell nuclei [121]. For example, for ^{24}Mg the experimental GDR is distributed over a range 16–18 MeV [121] compared with the calculations in Fig. 3 that have a range 16–26 MeV. Using an experimental centroid energy of 17 MeV together with our $B(E1)$ value would give $f_{\rm GDR} \approx 1.35$. The data used to obtained the parameters of the WBP and FSU Hamiltonians did not include the energy of the GDR. Thus, it is possible that the energy of the calculated energies of the GDR states could be modified by further adjustments of the potential and TBME parameters of the FSU Hamiltonian. It is also possible that the energy of the GDR is lowered and the width is increased by coupling with the continuum, which is not included in the calculations. Values of $f_{\rm GDR} \gg 1$ have generally been

[1]Such a broad and fragmented $B(E1; 0^+_1 \to 1^-_{\rm GDR})$ distribution for ^{24}Mg is supported by high-resolution measurements of the GDR region [121], where the fine structure is expected to arise from the deformation driven by α clustering. Albeit high-resolution data being also scarce, promising zero-degree (p, p') measurements at the required proton energies of $\gtrsim$200 MeV may soon become available for $A < 60$ nuclei through the PANDORA project [122].

associated with additional degrees of freedom arising from velocity-dependent interactions or short-range correlations—e.g., the aforementioned cluster formations—between protons and neutrons [18,90,123–127].

IV. CONCLUSIONS AND FURTHER WORK

This work explores the GDR and related electric dipole polarizability effects from SM calculations using the WBP and FSU interactions, and extend previous knowledge towards the end of the *sd* shell. Strong deviations from the hydrodynamic model are calculated following the smooth trend predicted independently by the leptodermous approximation using the FRDM model, and in agreement with calculations from first principles at shell closures. The sum of $E1$ strengths also follow a smooth, linear trend directly proportional to the mass number, which supports to some extent the complementary macroscopic nature of the GDR. Throughout, the classical oscillator strength sum rule is exceedingly exhausted by a factor of 1.5–2. The enhancement of the energy-weighted sum over $E1$ excitations with respect to the TRK sum rule comes from the use of realistic single-particle energies and the repulsive particle-hole interaction. The inclusion of missing admixtures with $1\hbar\omega$ 1p-1h + 2p-2h transitions may slightly suppress the $E1$ strength in closer agreement with photoabsorption cross-section measurements.

Further NCSM calculations of *sd*-shell nuclei up to $A = 24$ are now potentially available [128] and their results keenly expected; particularly using a new generation of χEFT non-local interactions and large $N_{\max}$ basis sizes [128]. Considerable experimental work is also required to accurately determine the currently scarce (γ, p) cross sections as well as the high-resolution structure of the GDR in order to benchmark the calculations presented here. More broadly, it will also be exciting to investigate the $E1$ polarizability of excited states [129] as well as unstable nuclei, where $\kappa(\text{g.s.}) = 1.26(10)$ remains the only data point corresponding to the ground state of the semimagic nucleus ^{68}Ni [27].

ACKNOWLEDGMENT

B.A.B. acknowledges National Science Foundation (NSF) Grant No. PHY-2110365.

[1] G. C. Baldwin and G. S. Klaiber, Phys. Rev. **71**, 3 (1947).
[2] A. B. Migdal, Zh. Eksp. Teor. Fiz. **15**, 81 (1945) [J. Phys. USSR **8**, 331 (1944)].
[3] M. Goldhaber and E. Teller, Phys. Rev. **74**, 1046 (1948).
[4] H. Steinwedel, J. H. D. Jensen, and P. Jensen, Phys. Rev. **79**, 1019 (1950).
[5] J. S. Levinger and D. C. Kent, Phys. Rev. **95**, 418 (1954).
[6] D. H. Wilkinson, Physica **22**, 1039 (1956).
[7] V. V. Balashov, Zh. Eksp. Teor. Fiz. **42**, 275 (1962).
[8] M. Danos and E. G. Fuller, Annu. Rev. Nucl. Sci. **15**, 29 (1965).
[9] C. F. v. Weizsäcker, Eur. Phys. J. A **96**, 431 (1935).
[10] H. A. Bethe and R. F. Bacher, Rev. Mod. Phys. **8**, 82 (1936).
[11] B. L. Berman and S. C. Fultz, Rev. Mod. Phys. **47**, 713 (1975).
[12] J. S. Levinger, Phys. Rev. **107**, 554 (1957).
[13] V. V. Flambaum, I. B. Samsonov, H. B. T. Tan, and A. V. Viatkina, Phys. Rev. A **103**, 032811 (2021).
[14] J. de Boer and J. Eichler, Adv. Nucl. Phys. **1**, 1 (1968).
[15] M. E. Rose, *Elementary Theory of Angular Momentum* (Wiley, New York, 1957).
[16] A. Messiah, *Quantum Mechanics* (North Holland Publishing Company, Amsterdam, 1961), Vols. 1 and 2.
[17] J. S. Levinger, *Nuclear Photo-Disintegration* (Oxford University Press, Oxford, 1960).
[18] A. B. Migdal, A. A. Lushnikov, and D. F. Zaretsky, Nucl. Phys. **66**, 193 (1965).
[19] S. S. Dietrich and B. L. Berman, At. Data Nucl. Data Tables **38**, 199 (1988).
[20] J. Ahrens, H. Gimm, A. Zieger, and B. Ziegler, Nuovo Cimento A **32**, 364 (1976).
[21] W. Knüpfer and A. Richter, Z. Phys. A: At. Nucl. (1975) **320**, 253 (1985).
[22] W. Knüpfer and A. Richter, Phys. Lett. B **107**, 325 (1981).
[23] V. A. Plujko, O. M. Gorbachenko, R. Capote, and P. Dimitriou, At. Data Nucl. Data Tables **123-124**, 1 (2018).
[24] T. Kawano, Y. S. Cho, P. Dimitriou, D. Filipescu, N. Iwamoto, V. Plujko, X. Tao, H. Utsunomiya, V. Varlamov, R. Xu *et al.*, Nucl. Data Sheets **163**, 109 (2020).
[25] B. S. Ishkhanov and I. M. Kapitonov, Phys. Usp. **64**, 141 (2021).
[26] J. N. Orce, At. Data Nucl. Data Tables **146**, 101511 (2022).
[27] D. M. Rossi, P. Adrich, F. Aksouh, H. Alvarez-Pol, T. Aumann, J. Benlliure, M. Böhmer, K. Boretzky, E. Casarejos, M. Chartier *et al.*, Phys. Rev. Lett. **111**, 242503 (2013).
[28] A. Tamii, I. Poltoratska, P. vonNeumann-Cosel, Y. Fujita, T. Adachi, C. A. Bertulani, J. Carter, M. Dozono, H. Fujita, K. Fujita, K. Hatanaka, D. Ishikawa, M. Itoh, T. Kawabata, Y. Kalmykov, A. M. Krumbholz, E. Litvinova *et al.*, Phys. Rev. Lett. **107**, 062502 (2011).
[29] X. Roca-Maza, X. Viñas, M. Centelles, B. K. Agrawal, G. Colo, N. Paar, J. Piekarewicz, and D. Vretenar, Phys. Rev. C **92**, 064304 (2015).
[30] T. Hashimoto, A. M. Krumbholz, P. G. Reinhard, A. Tamii, P. von Neumann-Cosel, T. Adachi, N. Aoi, C. A. Bertulani, H. Fujita, Y. Fujita, E. Ganioglu, K. Hatanaka, E. Ideguchi, C. Iwamoto, T. Kawabata, N. T. Khai, A. Krugmann *et al.* Phys. Rev. C **92**, 031305(R) (2015).
[31] X. Roca-Maza and N. Paar, Prog. Part. Nucl. Phys. **101**, 96 (2018).
[32] S. Bassauer, P. von Neumann-Cosel, P.-G. Reinhard, A. Tamii, S. Adachi, C. A. Bertulani, P. Y. Chan, G. Colò, A. D'Alessio, H. Fujioka *et al.*, Phys. Lett. B **810**, 135804 (2020).
[33] J. N. Orce, Int. J. Mod. Phys. E **29**, 2030002 (2020).
[34] R. Nathans and J. Halpern, Phys. Rev. **92**, 940 (1953).
[35] V. P. Denisov, L. A. Kul'chitskij, and I. Y. Chubukov, Izv. Akad. Nauk SSSR Seriya Fiz. **37**, 107 (1973).
[36] B. L. Berman, R. L. Bramblett, J. T. Caldwell, R. R. Harvey, and S. C. Fultz, Phys. Rev. Lett. **15**, 727 (1965).
[37] E. B. Bazhanov, A. P. Komar, A. V. Kulikov, and E. D. Makhnovsky, Nucl. Phys. **68**, 191 (1965).

[38] L. A. Kulchitskii, Y. M. Volkov, V. P. Denisov, and V. I. Ogurtsov, Ross. Akad. Nauk Ser. Fiz. **27**, 1412 (1963).

[39] R. L. Bramblett, B. L. Berman, M. A. Kelly, J. T. Caldwell, and S. C. Fultz, Photoneutron *Cross Sections* for ^{7}Li, edited by B. L. Berman, Tech. Rep. No. CONF—730301P1 (Lawrence Livermore Laboratory, University of California, United States, 1973).

[40] E. G. Fuller, Phys. Rep. **127**, 185 (1985).

[41] D. Zubanov, M. N. Thompson, B. L. Berman, J. W. Jury, R. E. Pywell, and K. G. McNeill, Phys. Rev. C **46**, 1147(E) (1992).

[42] J. W. Jury, B. L. Berman, D. D. Faul, P. Meyer, and J. G. Woodworth, Phys. Rev. C **21**, 503 (1980).

[43] J. G. Woodworth, K. G. McNeill, J. W. Jury, R. A. Alvarez, B. L. Berman, D. D. Faul, and P. Meyer, Phys. Rev. C **19**, 1667 (1979).

[44] P. D. Allen, E. G. Muirhead, and D. V. Webb, Nucl. Phys. A **357**, 171 (1981).

[45] A. N. Gorbunov, V. A. Dubrovina, V. A. Osipova, V. S. Silaeva, and P. A. Cerenkov, Sov. Phys. J. Exp. Theor. Phys. **15**, 520 (1962).

[46] V. V. Varlamov, B. S. Ishkhanov, I. M. Kapitonov, V. I. Shvedunov, and Y. I. Prokopchuk, Yad. Fiz. (USSR) **30** (1979).

[47] D. W. Anderson, B. C. Cook, and T. J. Englert, Nucl. Phys. A **127**, 474 (1969).

[48] M. Miorelli, S. Bacca, N. Barnea, G. Hagen, G. R. Jansen, G. Orlandini, and T. Papenbrock, Phys. Rev. C **94**, 034317 (2016).

[49] J. N. Orce, T. E. Drake, M. K. Djongolov, P. Navrátil, S. Triambak, G. C. Ball, H. AlFalou, R. Churchman, D. S. Cross, P. Finlay, C. Forssen, A. B. Garnsworthy, P. E. Garrett, G. Hackman, A. B. Hayes, R. Kshetri *et al.*, Phys. Rev. C **86**, 041303(R) (2012).

[50] M. Kumar-Raju, J. N. Orce, P. Navrátil, G. C. Ball, T. E. Drake, S. Triambak, G. Hackman, C. J. Pearson, K. J. Abrahams, E. H. Akakpo *et al.*, Phys. Lett. B **777**, 250 (2018).

[51] P. Möller, J. R. Nix *et al.*, At. Data Nucl. Data Tables **66**, 131 (1997).

[52] J. Gibelin, D. Beaumel, T. Motobayashi, Y. Blumenfeld, N. Aoi, H. Baba, Z. Elekes, S. Fortier, N. Frascaria, N. Fukuda *et al.*, Phys. Rev. Lett. **101**, 212503 (2008).

[53] N. Paar, D. Vretenar, E. Khan, and G. Colo, Rep. Prog. Phys. **70**, R02 (2007).

[54] P. von Neumann-Cosel, Phys. Rev. C **93**, 049801 (2016).

[55] N. Arsenyev, A. Severyukhin, V. Voronov, and N. Van Giai, EPJ Web of Conf. **107**, 05006 (2016).

[56] B. C. Cook, Phys. Rev. **106**, 300 (1957).

[57] R. A. Eramzhyan, B. S. Ishkhanov, I. M. Kapitonov, and V. G. Neudatchin, Phys. Rep. **136**, 229 (1986).

[58] S. Nakayama, T. Yamagata, H. Akimune, I. Daito, H. Fujimura, Y. Fujita, M. Fujiwara, K. Fushimi, M. B. Greenfield, H. Kohri, N. Koori, K. Takahisa, A. Tamii, M. Tanaka, and H. Toyokawa, Phys. Rev. Lett. **87**, 122502 (2001).

[59] O. Burda, P. von Neumann-Cosel, A. Richter, C. Forssén, and B. A. Brown, Phys. Rev. C **82**, 015808 (2010).

[60] T. Aumann, A. Leistenschneider, K. Boretzky, D. Cortina, J. Cub, W. Dostal, B. Eberlein, Th. W. Elze, H. Emling, H. Geissel *et al.*, Nucl. Phys. A **649**, 297 (1999).

[61] A. Leistenschneider, T. Aumann, K. Boretzky, D. Cortina, J. Cub, U. D. Pramanik, W. Dostal, T. W. Elze, H. Emling, H. Geissel *et al.*, Phys. Rev. Lett. **86**, 5442 (2001).

[62] J. Terasaki and J. Engel, Phys. Rev. C **74**, 044301 (2006).

[63] A. Bürger, A. C. Larsen, S. Hilaire, M. Guttormsen, S. Harissopulos, M. Kmiecik, T. Konstantinopoulos, M. Krtička, A. Lagoyannis, T. Lönnroth *et al.*, Phys. Rev. C **85**, 064328 (2012).

[64] A. C. Larsen, M. Guttormsen, R. Chankova, F. Ingebretsen, T. Lönnroth, S. Messelt, J. Rekstad, A. Schiller, S. Siem, N. U. H. Syed *et al.*, Phys. Rev. C **76**, 044303 (2007).

[65] A.-C. Larsen, A. Spyrou, S. N. Liddick, and M. Guttormsen, Prog. Part. Nucl. Phys. **107**, 69 (2019).

[66] J. E. Midtbø, F. Zeiser, E. Lima, A.-C. Larsen, G. M. Tveten, M. Guttormsen, F. L. B. Garrote, A. Kvellestad, and T. Renstrøm, Comput. Phys. Commun. **262**, 107795 (2021).

[67] A. Zilges, D. L. Balabanski, J. Isaak, and N. Pietralla, Prog. Part. Nucl. Phys. **122**, 103903 (2022).

[68] C. Ngwetsheni and J. N. Orce, Phys. Lett. B **792**, 335 (2019).

[69] C. Ngwetsheni and J. N. Orce, Hyperfine Interact. **240**, 94 (2019).

[70] C. Ngwetsheni and J. N. Orce, EPJ Web Conf. **223**, 01045 (2019).

[71] J. N. Orce, Phys. Rev. C **91**, 064602 (2015).

[72] J. N. Orce, Phys. Rev. C **93**, 049802 (2016).

[73] EXFOR: Experimental nuclear reaction data, https://www-nds.iaea.org/exfor/exfor.htm, accessed 2022-05-21.

[74] ENDF: Evaluated nuclear data file, https://www-nds.iaea.org/exfor/endf.htm, accessed 2022-05-21.

[75] B. I. Goryachev, B. S. Ishkhanov, I. M. Kapitonov, I. M. Piskarev, O. P. Shevchenko, and V. G. Shevchenko, Yad. Fiz. **7**, 944 (1968) [Sov. J. Nucl. Phys. **7**, 567 (1968)].

[76] B. I. Goryachev, B. S. Ishkhanov, V. G. Shevchenko, and B. A. Yurev, Yad. Fiz. **7**, 1168 (1968) [Sov. J. Nucl. Phys. **7**, 698 (1968).

[77] P. Navrátil, Few-Body Syst. **41**, 117 (2007).

[78] R. Roth, A. Calci, J. Langhammer, and S. Binder, Phys. Rev. C **90**, 024325 (2014).

[79] D. R. Entem and R. Machleidt, Phys. Rev. C **68**, 041001(R) (2003).

[80] D. R. Entem, R. Machleidt, and Y. Nosyk, Phys. Rev. C **96**, 024004 (2017).

[81] D. R. Entem, N. Kaiser, R. Machleidt, and Y. Nosyk, Phys. Rev. C **91**, 014002 (2015).

[82] S. K. Bogner, R. J. Furnstahl, and R. J. Perry, Phys. Rev. C **75**, 061001 (2007).

[83] I. Stetcu, S. Quaglioni, J. L. Friar, A. C. Hayes, and P. Navrátil, Phys. Rev. C **79**, 064001 (2009).

[84] B. Brown, A. Etchegoyen, W. Rae, and N. Godwin, MSU-NSCL Report **524** (1988).

[85] E. K. Warburton and B. A. Brown, Phys. Rev. C **46**, 923 (1992).

[86] R. S. Lubna, K. Kravvaris, S. L. Tabor, V. Tripathi, A. Volya, E. Rubino, J. M. Allmond, B. Abromeit, L. T. Baby, and T. C. Hensley, Phys. Rev. C **100**, 034308 (2019).

[87] R. S. Lubna, K. Kravvaris, S. L. Tabor, V. Tripathi, E. Rubino, and A. Volya, Phys. Rev. Res. **2**, 043342 (2020).

[88] B. A. Brown, Physics (Basel) **4**, 525 (2022).

[89] B. A. Brown and W. A. Richter, Phys. Rev. C **74**, 034315 (2006).

[90] J. S. Levinger and H. A. Bethe, Phys. Rev. **78**, 115 (1950).

[91] E. K. Warburton and J. Weneser, in *Isospin in Nuclear Physics*, edited by D. H. Wilkinson (North-Holland, Amsterdam, 1969), Chap. 5.

[92] A. N. Bohr and B. R. Mottelson, *Nuclear Structure* (World Scientific Publishing Company, Singapore, 1998), Vols. 1 and 2.
[93] H. Morinaga, Phys. Rev. **97**, 444 (1955).
[94] F. C. Barker and A. K. Mann, Philos. Mag. (1798–1977) **2**, 5 (1957).
[95] K. Sieja, Dipole excitations in nuclei: Recent configuration interaction studies, presented at *Giant and Soft Modes of Excitation in Nuclear Structure and Astrophysics, ECT** (2022).
[96] K. Sieja, Eur. Phys. J. A **59**, 147 (2023).
[97] D. H. Gloeckner and R. D. Lawson, Phys. Lett. B **53**, 313 (1974).
[98] B. A. Brown, Natl. Super Conduct. Cyclotr. Lab. **11** (2005).
[99] V. Neudatchin, Y. F. Smirnov, and N. Golovanova, Adv. Nucl. Phys. **11**, 1 (1979).
[100] W. B. He, Y. G. Ma, X. G. Cao, X. Z. Cai, G. Q. Zhang *et al.*, Phys. Rev. Lett. **113**, 032506 (2014).
[101] U. Smilansky, B. Povh, and K. Traxel, Phys. Lett. B **38**, 293 (1972).
[102] A. Weller, P. Egelhof, R. Čaplar, O. Karban, D. Krämer, K.-H. Möbius, Z. Moroz, K. Rusek, E. Steffens, G. Tungate *et al.*, Phys. Rev. Lett. **55**, 480 (1985).
[103] F. C. Barker and C. L. Woods, Aust. J. Phys. **42**, 233 (1989).
[104] F. C. Barker, Aust. J. Phys. **37**, 267 (1984).
[105] K. Ikeda, N. Takigawa, and H. Horiuchi, Prog. Theor. Phys. Suppl. **E68**, 464 (1968).
[106] Y. Kanada-En'yo and H. Horiuchi, Prog. Theor. Phys. **93**, 115 (1995).
[107] W. von Oertzen, M. Freer, and Y. Kanada-En'yo, Phys. Rep. **432**, 43 (2006).
[108] M. Freer, Rep. Prog. Phys. **70**, 2149 (2007).
[109] J.-P. Ebran, E. Khan, T. Nikšić, and D. Vretenar, Nature (London) **487**, 341 (2012).
[110] B. Zhou, Z. Ren, C. Xu, Y. Funaki, T. Yamada, A. Tohsaki, H. Horiuchi, P. Schuck, and G. Röpke, Phys. Rev. C **86**, 014301 (2012).
[111] J. A. Kuehner, R. H. Spear, W. J. Vermeer, M. T. Esat, A. M. Baxter, and S. Hinds, Phys. Lett. B **115**, 437 (1982).
[112] J. Tian, H. Cui, K. Zheng, and N. Wang, Phys. Rev. C **90**, 024313 (2014).
[113] W. D. Myers and W. J. Swiatecki, Ann. Phys. (NY) **55**, 395 (1969).
[114] P. Möller, A. J. Sierk, T. Ichikawa, and H. Sagawa, At. Data Nucl. Data Tables **109-110**, 1 (2016).
[115] W. Thomas, Naturwissenschaften **13**, 627 (1925).
[116] R. Ladenburg and F. Reiche, Naturwissenschaften **11**, 584 (1923).
[117] F. Reiche and W. Thomas, Eur. Phys. J. A **34**, 510 (1925).
[118] W. Kuhn, Eur. Phys. J. A **33**, 408 (1925).
[119] G. F. Bertsch, *The Practitioner's Shell Model* (North Holland Publishing Company, Amsterdam, 1972).
[120] J. Blomqvist and A. Molinari, Nucl. Phys. A **106**, 545 (1968).
[121] R. W. Fearick, B. Erler, H. Matsubara, P. von Neumann-Cosel, A. Richter, R. Roth, and A. Tamii, Phys. Rev. C **97**, 044325 (2018).
[122] A. Tamii, L. Pellegri, P.-A. Söderström, D. Allard, S. Goriely, T. Inakura, E. Khan, E. Kido, M. Kimura, E. Litvinova *et al.*, arXiv:2211.03986.
[123] M. Ferentz, M. Gell-Mann, and D. Pines, Phys. Rev. **92**, 836 (1953).
[124] M. H. Johnson and E. Teller, Phys. Rev. **98**, 783 (1955).
[125] V. F. Weisskopf, Nucl. Phys. **3**, 423 (1957).
[126] S. Rand, Phys. Rev. **107**, 208 (1957).
[127] W. Brenig, K. A. Brueckner (Ed.), *Advances in Theoretical Physics* (Academic Press, NY, 1965), Vol. 1, p. 59.
[128] C. Sarma and P. C. Srivastava, J. Phys. G: Nucl. Part. Phys. **50**, 045105 (2023).
[129] J. Eichler, Phys. Rev. **133**, B1162 (1964).